J Comput Neurosci (2011) 31:229–245
DOI 10.1007/s10827-010-0310-z

Topologically invariant macroscopic statistics in balanced networks of conductance-based integrate-and-fire neurons

Pierre Yger · Sami El Boustani · Alain Destexhe · Yves Frégnac

Received: 28 November 2009 / Revised: 26 October 2010 / Accepted: 20 December 2010 / Published online: 11 January 2011

Abstract The relationship between the dynamics of neural networks and their patterns of connectivity is far from clear, despite its importance for understanding functional properties. Here, we have studied sparsely-connected networks of conductance-based integrate-and-fire (IF) neurons with balanced excitatory and inhibitory connections and with finite axonal propagation speed. We focused on the genesis of states with highly irregular spiking activity and synchronous firing patterns at low rates, called slow Synchronous Irregular (SI) states. In such balanced networks, we examined the "macroscopic" properties of the spiking activity, such as ensemble correlations and mean firing rates, for different intracortical connectivity profiles ranging from randomly connected networks to networks with Gaussian-distributed local connectivity. We systematically computed the distance-dependent correlations at the extracellular (spiking) and intracellular (membrane potential) levels between randomly assigned pairs of neurons. The main finding is that such properties, when they are averaged at a macroscopic scale, are invariant with respect to the different connectivity patterns, provided the excitatory-inhibitory balance is the same. In particular, the same correlation structure holds for different connectivity profiles. In addition, we examined the response of such networks to external input, and found that the correlation landscape can be modulated by the mean level of synchrony imposed by the external drive. This modulation was found again to be independent of the external connectivity profile. We conclude that first and second-order "mean-field" statistics of such networks do not depend on the details of the connectivity at a microscopic scale. This study is an encouraging step toward a mean-field description of topological neuronal networks.

Keywords Topological networks · Mean-field · Correlation · Synchrony · Intracortical connectivity

Action Editor: Mark van Rossum

Pierre Yger and Sami El Boustani contributed equally.

Electronic supplementary material The online version of this article (doi:10.1007/s10827-010-0310-z) contains supplementary material, which is available to authorized users.

P. Yger · S. El Boustani · A. Destexhe (✉) · Y. Frégnac
Unité de Neuroscience Information et Complexité (UNIC), UPR 3293 CNRS, Bat. 32-33, 1 Avenue de la Terrasse, 91198 Gif-sur-Yvette, France
e-mail: destexhe@unic.cnrs-gif.fr

1 Introduction

Spatio-temporal correlations are a key signature of the cortical population spiking discharge, measured in the recurrent spontaneous ongoing activity or from sensory-driven activity. Correlations have been classically considered as a crucial component of the neuronal assembly code (Singer and Gray 1995; Nirenberg and Latham 2003) also linked to behavior (Zohary et al. 1994). Today, a more precise insight about their spatiotemporal structure, at the supra- and/or subthreshold level, is given by analysis techniques using intracellular recordings and modeling (Destexhe and Paré 1999; El Boustani et al. 2009), multi electrode arrays (Smith and Kohn 2008), or 2-photon imaging (Göbel et al. 2007; Greenberg et al. 2008). Understanding how these correlations emerge in recurrent

neuronal networks and how their structure could be related to generic network properties can help in assessing their functional role and their relation to or independence with the local microscopic anatomical connectivity.

One important issue about neuronal correlations lies in the way they are modulated by external stimulation. It is well known that neuronal pairwise correlations can be affected by the presentation of a stimulus (Kohn and Smith 2005; Nauhaus et al. 2009; Smith and Kohn 2008; Mitchell et al. 2009), but the way they change as a function of the stimulus statistics is poorly understood. Identifying the generic properties of the input that can influence the pairwise cross-correlation profile within sensory areas could provide an estimation of the sensory input properties knowing some experimental functional measurements.

In the superficial layers of the primary visual cortex, correlations are clustered as a function of the underlying orientation maps constraining the correlated inputs that are more frequently seen by a particular neuron (Berger et al. 2007; Nauhaus et al. 2009) but they can also span a large cortical surface (Smith and Kohn 2008; Schwarz and Bolz 1991) decaying with distance. In this context, the distance-dependent profile of pairwise cross-correlations could be used to gain some knowledge about the underlying anatomical/hard-wired connectivity.

The balanced random network (van Vreeswijk and Sompolinsky 1996, 1998; Brunel 2000; Vogels and Abbott 2005; Kumar et al. 2008; El Boustani and Destexhe 2009; Amit and Brunel 1997; Renart et al. 2010) is a commonly used and convenient framework to study the dynamics of large-scale populations of sparsely-connected integrate-and-fire neurons, and to reproduce the so-called slow Synchronous Irregular (SI) regime (Brunel 2000). In this regime, neurons fire in an irregular manner, behaving almost like Poisson processes, and the average pairwise cross-correlation value is modulated by the internal balance and the external input. This regime is well suited to produce slow oscillations reminiscent of those observed *in vivo* (Han et al. 2008; Arieli et al. 1996). In such models, analytical techniques can be used to study the distributions of the pairwise cross-correlations for some topological profiles and network regimes (Kriener et al. 2009).

However, despite its generality, this classical model with random connectivity lacks several important biological features ignored because they complexify the analytical approach to the problem. In this paper, we chose to study a more realistic two-dimensional network of integrate-and-fire neurons, which is more relevant biologically since it includes propagation delays (Bringuier et al. 1999; Benucci et al. 2007) and conductance-based synapses (Vogels and Abbott 2005; Cessac and Viéville 2008; Kumar et al. 2008; Marre et al. 2009). We provide a detailed numerical study of its spatio-temporal correlations for Gaussian connectivity profiles, previously introduced in the context of information processing (Mehring et al. 2003). Such a model is a minimal model for capturing propagation phenomena which can be directly observed *in vivo* with large scale recordings (voltage-sensitive dye imaging, multi electrode recording, 2-photon imaging).

In the first part, we study the organization of the pairwise cross-correlations as a function of distance in generic 2D networks of integrate-and-fire neurons subject to unstructured input, a case that will be referred to as the spontaneous activity case. This irregular but tonic bombardment is supposed to simulate the effect of the retinal "dark discharge" in thalamocortical visual networks, which is detected in the absence of any visual drive. We characterize correlation profiles as a function of the distance between pairs of neurons and their sensitivity when varying key parameters of the microscopic network structure. In the second part of the paper, we study the behavior of the same network when driven with synchronous inputs, to study how the profile of its pairwise cross-correlations is affected.

2 Materials and methods

Neuron model The simulated networks were composed of $N = 12{,}500$ (10,000 excitatory and 2,500 inhibitory) conductance-based leaky integrate-and-fire neurons with a membrane time constant $\tau_m = 20$ ms, a leak conductance $G_{leak} = 10$ nS, and a resting membrane potential $V_{rest} = -80$ mV. When the membrane potential V_m reaches the spiking threshold $V_{thresh} = -50$ mV, a spike is generated and the membrane potential is clamped to the reset potential $V_{reset} = -60$ mV during a refractory period of duration $\tau_{ref} = 5$ ms. These parameters were kept fixed and were chosen as biologically plausible and in line with previous studies. Only the refractory period τ_{ref} was varied in additional simulations to be sure that the results found, based on instantaneous cross-correlations, were not qualitatively affected by this value. Others simulations were also performed to check the validity of the result with larger networks up to 100,000 neurons.

Synapse model The synaptic interactions between these neurons were modeled as transient conductance changes. The synaptic time course was modeled as an instantaneous rise followed by an exponential decay.

The synaptic time constants were chosen to be $\tau_{\text{exc}} = 3$ ms and $\tau_{\text{inh}} = 7$ ms for excitation and inhibition respectively. The reversal potentials were $E_{\text{exc}} = 0$ mV and $E_{\text{inh}} = -70$ mV.

The complete set of equations describing the dynamics of a neuron is thus

$$\tau_{\text{m}} \frac{\text{d}\, V(t)}{dt} = (V_{\text{rest}} - V(t)) + g_{\text{exc}}(t)(E_{\text{exc}} - V(t)) + g_{\text{inh}}(t)(E_{\text{inh}} - V(t))$$

$$\tau_{\text{syn}} \frac{\text{d}\, g_{\text{syn}}(t)}{dt} = -g_{\text{syn}}(t) + S_{\text{syn}}(t)$$

where syn $\in$ {exc, inh}, $S_{\text{syn}}(t) = \sum_{i,k} \delta(t - t_i^k)$ are the incoming synaptic spike trains where $i \in \{1, .., N\}$ refers to presynaptic neurons and k to the different spike times of these neurons. Here $g_{\text{syn}}(t)$ is expressed in units of the leak conductance. In this paper, we used 4nS for the excitatory conductance, and a balance of $g = 16$ unless stated otherwise. The main parameters are summarized in Table 1.

Spatial organization A cortical area of $L = 1$ mm^2 was simulated as a 2D-layer-like network with periodic boundary conditions and an excitatory/inhibitory neuron number ratio of 4:1. Note that since the density of neurons is arbitrarily selected, and since it varies between species and cortical areas (Braitenberg and Schüz 1998), this value of 1 mm^2 should not be taken as realistic. This scale is more in the order of a V1 hypercolumn where local circuits prevail and long-range horizontal connections are not included, being beyond the network size. It is therefore distinct from the larger scale usually used in neural mass models. Neurons were arranged on a grid, and even though such a regular structure may slightly bias the connectivity (Voges et al. 2007), we checked with additional simulations that the results remained the same if neurons were drawn uniformly across the layer. Every neuron was sparsely connected with the rest of the network with a connection probability that depended on the distance r_{ij} between two neurons in the network according to a Gaussian profile:

$$p_{ij} = e^{-\frac{r_{ij}^2}{2\sigma_c^2}} \tag{1}$$

where σ_c^2 is the variance of the connectivity profile, i.e. the spatial spread of the Gaussian profile. For each neuron, $K = \epsilon N$ incoming connections were drawn by randomly picking other neurons in the network that will or not create a projection according to a rejection method based on the Gaussian profile. ϵ is defined as the connection density. The total number K of synapses per neuron was fixed, so whatever the σ_c value, each neuron kept the same number of incoming synapses for the sake of comparability. Two connection densities were mainly studied: a highly sparse one (with a connection density $\epsilon = 0.5\%$) and a denser one (with $\epsilon = 5\%$).

The neuron density in the network being uniform and connections being restricted to the maximal value $L/\sqrt{2}$, the probability of finding one neuron at distance r equals:

$$P(r) = \begin{cases} \dfrac{2\pi r}{L^2} & \text{if } r \le L/2 \\ \dfrac{r(2\pi - 8\arccos(L/(2r))}{L^2} & \text{if } L/2 < r \le L/\sqrt{2} \\ 0 & \text{if } L/\sqrt{2} < r \end{cases} \tag{2}$$

The number of actually established connections at a distance r, where the distance-dependent connection probability is given by the Gaussian profile, is thus:

$$N_{\text{realized}}(r) = N P(r) \exp(-r^2/2\sigma_c^2) \tag{3}$$

with the normalization condition $\int_0^{L/\sqrt{2}} N_{\text{realized}}(r)dr = \epsilon N$. In the network, the probability of connection is therefore $\rho(r) = P(r)\exp(-r^2/2\sigma_c^2)$ such that $\int_0^{L/\sqrt{2}} \rho(r)dr = \epsilon$.

The network was considered to be in a spontaneous state when an unstructured and stationary external input was fed into it. In the case where the local network was stimulated, another excitatory layer-like network projected onto the cortical network in a topological manner, described by another Gaussian distribution with variance σ_{ext}^2. The total number of external

Table 1 Parameter table summarizing all the cells and network parameters used in the simulations

τ_{m}	20 ms
τ_{ref}	5 ms
τ_{exc}	3 ms
τ_{inh}	7 ms
V_{rest}	−80 mV
V_{thresh}	−50 mV
V_{reset}	−60 mV
E_{exc}	0 mV
E_{inh}	−70 mV
G_{leak}	10 nS
Δg_{exc}	4 nS
Δg_{inh}	16 $\Delta g_{\text{exc}} = 64$ nS
d_{syn}	0.2 ms
v	0.2 m.s^{-1}
simtime	5,500 s
ϵ	0.5%, 5%
σ_c	[50, 1,000] μm

synapses received by each neuron was the same as K, the number of recurrent synapses.

Delays We used non-homogeneous delays which depended linearly on the distances r_{ij} through

$$d_{ij} = d_{\text{syn}} + \frac{r_{ij}}{v}$$

where the value of v was taken from the literature. A value of 0.1–0.5 m/s is usually reported (Bringuier et al. 1999; Gonzlez-Burgos et al. 2000), and in all simulations, we used $v = 0.2$ m/s, and $d_{\text{syn}} = 0.2$ ms.

Simulator All simulations were performed using the NEST simulator (Diesmann and Gewaltig 2001) and the PyNN interface (Davison et al. 2009). Correlated input in the external layer was built by combining Poisson processes and the processes generated with the Multiple Interaction Process (MIP) algorithm (Kuhn et al. 2003).

Data analysis Since the maximal distance between two neurons in our network is $\frac{\sqrt{2}}{2} \simeq 0.7$ mm, we divided the spatial domain into slices of width $w = 50$ μm. Spike trains were digitized with a time bin equal to the refractory period of the neurons, i.e. 5 ms, and for each slice we selected $N = 2{,}000$ pairs of neurons before averaging the Pearson correlation coefficients (CC) computed over all these pairs. The spatial profile of the correlation is therefore given by the following function $f(r) = \langle CC(r) \rangle$ where $\langle CC(r) \rangle$ is the average Pearson coefficient correlation over $N = 2{,}000$ pairs of cells separated by a distance r. Cells that remained silent during the simulations were discarded from the analysis, and spiking data were gathered during 5 s of stationary simulation. For the subthreshold activity, we selected a row of neurons in the network and we computed the instantaneous cross-correlation for each pair as a function of distance. The resulting function was characterized by computing its integral value over distance ('Integrated correlation') and its linear slope in a log-log representation ('Scaling exponent of the correlation') (see Fig. 5). Integrated correlation can therefore be defined as:

$$\langle IC \rangle = \int_0^{\frac{L}{\sqrt{2}}} f(r)dr \tag{4}$$

The integrated correlation is related to the global synchrony in the network, $\langle CC \rangle$, by the relationship $\langle CC \rangle = \int_0^{\frac{L}{\sqrt{2}}} P(r)\, f(r)dr$, where $P(r)$ is the probability of finding pairs of cells spaced by a distance r. This definition is convenient for avoiding the bias produced by boundary conditions as shown in Fig. 1(a). For the network activity spike-triggered average, we randomly sampled 100 neurons for which the average was computed over the whole spike train ensemble.

3 Topological network model

Cortical connectivity is still poorly understood, but is definitely not as random as was usually modeled in previous studies. Whether the connectivity graph is small-world (the definition is ambiguous when con-

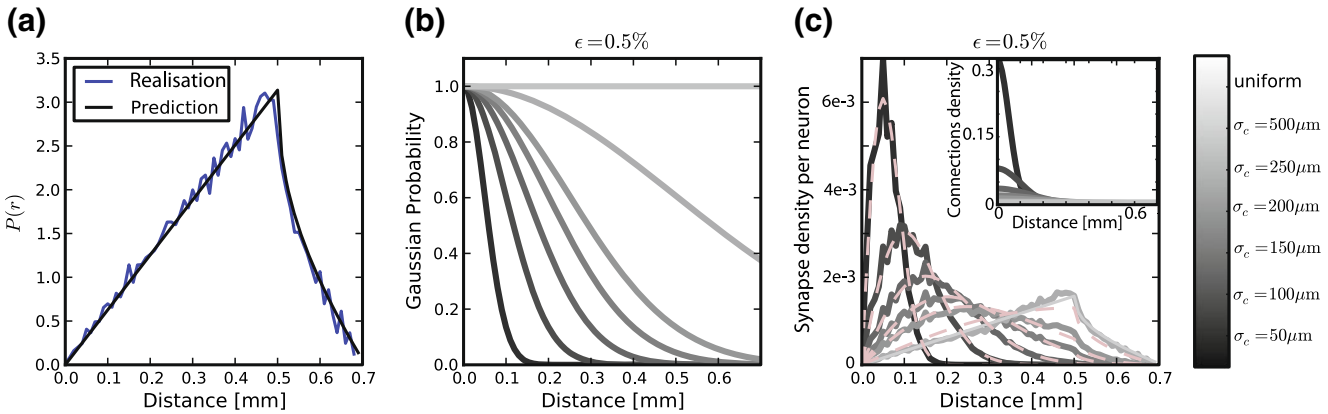

Fig. 1 Profile of the connections. (**a**) Distribution $P(r)$ of interneuron distances from one excitatory cell to all the other cells in the network, from Eq. (2). The kink at 0.5 mm is due to the finite size of the network. (**b**) Profile of the Gaussian kernels used to draw the connections, for various σ_c. (**c**) Probability of established synapses as a function of the distance between neurons in the network for $\epsilon = 0.5\%$, for several values of the connection spread, σ_c. The corresponding mean values are represented as *dotted lines*, and the analytical predictions are plotted in *dash dotted black lines*. The *solid black line* shows the control case of a purely random network. The *inset* in panel C shows the Gaussian profiles of the connectivity when normalization condition is taken into account

sidering propagation delays), clustered, or Gaussian is still unclear, but biological evidence shows that neurons in the cortex project mainly to their surroundings (Hellwig 2000; Bienenstock 1996). As a first approximation, neurons can be considered as being connected with a distance-dependent probability following a Gaussian profile. Even though it is known that real connectivity is less isotropic and homogeneous (for example the orientation maps and the patchy horizontal connectivity in V1 (Gilbert and Wiesel 1983)), the Gaussian profile is a good description of a small cortical area where long-range interactions are ignored. Therefore, every neuron in our model is connected with the rest of the network with a 2D Gaussian probability function and a fixed number of incoming synapses, while periodic boundary conditions are used throughout the study to avoid any boundary effects. In order to obtain *in vivo*-like states, we adopted the usual integrate-and-fire balanced network configuration comprising a 4:1 ratio between excitatory and inhibitory neurons (Brunel 2000). The synaptic weights were chosen in order to obtain balanced subthreshold fluctuating dynamics responsible for the irregular firing.

Propagation delays are known to lead to a large diversity of states in large-scale neuronal networks (Roxin et al. 2005; Izhikevich et al. 2004). While they are often discarded in large-scale models, under the assumption that they can be neglected in a small cortical area, biological studies (Bringuier et al. 1999; Gonzlez-Burgos et al. 2000) have reported typical values of 0.1–0.5 m/s for conduction delays, and comparable values can be observed in voltage sensitive dye imaging, where activity waves propagate at a similar speed (Grinvald et al. 1994; Benucci et al. 2007; Nauhaus et al. 2009). Patch recordings *in vitro* confirm that these delays scale linearly as a function of distance (Larkum et al. 2001) when considering the propagation from dendrites to the soma. Thus, even for a small patch of cortex of 1 mm^2, with a synaptic delay of 0.2 ms (due to neurotransmitter release), conduction delays are broadly distributed and should not be neglected. Moreover artificial oscillations can arise in networks where delays are homogeneous (Brunel 2000). Our network was therefore built as an artificial square lattice of 1 mm^2 and we chose a propagation speed of $v = 0.2$ m/s.

Figure 1(c) shows the distribution of the distances in the network as a function of the Gaussian spread σ_c. The case of an equivalent uniform distribution is added for comparison ($\sigma_c = \infty$). By construction, the distributions of $\rho(r)$ are continuously affected by σ_c, and are not Gaussian. Indeed, these functions are the product of the Gaussian profiles of connectivity (see Fig. 1(b)) and the probability $P(r)$ of finding a pair of neuron for a given distance under the normalization condition $\int_0^{L/\sqrt{2}} P(r)\exp(-r^2/2\sigma_c^2)dr = \epsilon$ (see Fig. 1(c) for the case $\epsilon = 0.5\%$). The inset in Fig. 1(c) shows the effective probability of connections between neurons under this normalization condition. The case $\epsilon = 5\%$ can be obtained by scaling the curves in Fig. 1(c) by a factor 10.

During the so-called spontaneous activity, every neuron in the network is stimulated with decorrelated Poisson input. Even if in terms of numbers of synapses the synaptic drive of cortical neurons in V1 originates mainly from the recurrent network, the efficacy of the feedforward thalamocortical synapses is the largest (Gil et al. 1999). To simulate the functional balance between recurrent and feedforward input, each neuron in the cortical layer received the same number of external synapses as recurrent ones. When we considered correlated input, an external layer was added on top of the network where external units produced synchronous Poisson spike trains projecting on a subset of the 2D network with Gaussian probability distributions. There were no delays from the stimulation layer to the recurrent network layer.

4 Response under unstructured noise

In the spontaneous activity regime, i.e. when uncorrelated Poisson external noise was applied to all the synapses at a mean frequency of $\nu_{\text{ext}} = 5$ spikes/s, the network displayed waves emerging in random places which tended to propagate all over the surface. It should be noted that such networks are not able to maintain self-sustained activity by themselves. Several studies previously reported that these ongoing and reverberating regimes could be observed in networks with conductance-based synapses (Vogels and Abbott 2005; Kumar et al. 2008; El Boustani and Destexhe 2009; Marre et al. 2009), but they were all achieved in networks without any propagation delays. We empirically noticed that the linear propagation time taken into account here (see Section 2) increases the average synaptic delay and therefore the neuron density that would have been necessary to observe such a spontaneous regime. The average delay within the present network is close to 0.75 ms for $\sigma_c = 100$ μm, and depends on σ_c (see Fig. 1(c), since the delay is linearly related to distance). Nevertheless, it has been shown that a weak uncorrelated external input does not alter the main statistical features of these models (Brunel 2000; Vogels and Abbott 2005) and their irregular activ-

ity could not be completely explained by the stochastic nature of this background activity, such that we can still study the interplay between spontaneous and evoked correlated activity.

As can be seen in Fig. 2, large sub-threshold waves developed at the conductance level. Waves of excitation, popping up at random places, were immediately followed by an increase of inhibition, traveling simultaneously across the network due to the connection rule and the delays. These waves are reflected in the supra- and sub-threshold activity usually experimentally recorded (Han et al. 2008; Nauhaus et al. 2009).

To gain some insights into the role of the network structure, we varied in a systematic manner two main parameters : the spatial extent of the Gaussian profile used for the recurrent connections σ_c and the balance between excitatory and inhibitory synaptic strength g. The results are shown in Fig. 3, for two different connectivity densities, $\epsilon \in \{0.5\%, 5\%\}$. The first striking observation is that for both connection densities, averaged quantities such as the mean firing rate and the mean coefficient of variation of the inter-spike interval (CV ISI) do not depend on the connectivity spread σ_c but are controlled only by the balance g between excitation and inhibition (see Fig. 3(a, b, e, f)). A similar result has been previously observed in El Boustani and Destexhe (2009). At the population level, the only relevant parameters for these macroscopic quantities are therefore the average number of synapses received per neuron and their strength, not the precise layout of the recurrent connectivity. There is somehow a match between the level at which simple anatomical details should be taken into account and the scale of measurement. Of course, this is true as long as the connections are sparse enough: in the limit case of very small σ_c, we are almost in a nearest-neighbors situation and the local correlations are too strong to keep averaged quantities invariant. This is an extreme situation where usual mean-field models are not valid anymore.

The second result concerns the irregular and oscillatory nature of the dynamics. Typical raster plots of the observed activity regime (Fig. 3(d, h), $g = 16$ and $\sigma_c = 100$ μm) show low-rate irregular firing, with an oscillatory activity made of spontaneous waves (see also Fig. 2). Within these waves, neurons fire irregularly with a mean CV ISI close to one, while the frequency of these oscillations is only slightly affected by σ_c (Fig. 3(c, g)). Nevertheless, one can observe that by increasing the connectivity density, the influence of σ_c on the frequency tends to increase. So, for highly connected network, one would expect a more significant impact of the connectivity on the network oscillations.

The network state depends on the balance g between excitation and inhibition, and on the frequency of the external noise ν_{ext}. Several regimes can be observed,

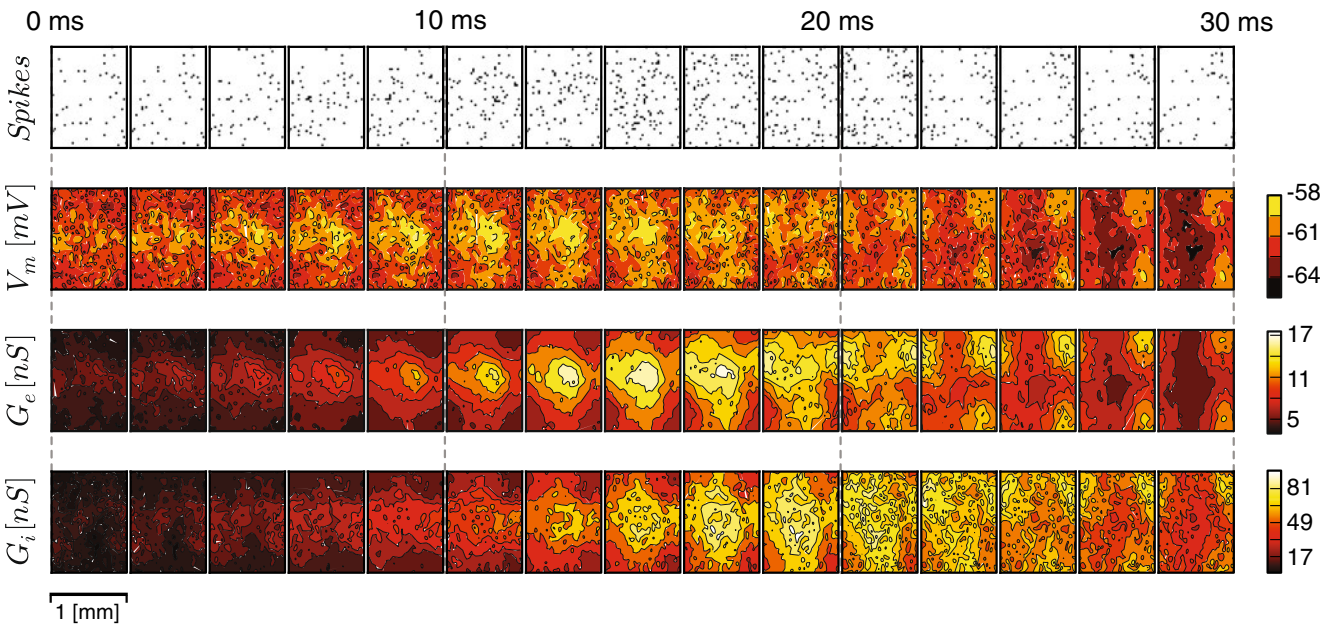

Fig. 2 Snapshots of the spontaneous ongoing activity in the 2D network. Neuronal responses at the supra-threshold (spikes) and sub-threshold (V_m) levels for every neuron in the 2D network are shown in the top and second rows, respectively. Snapshots are taken every 2 ms for a total duration of 28 ms. The last two rows show instantaneous input conductance maps. Excitatory conductances are represented in the third row and the inhibitory conductances in the last row

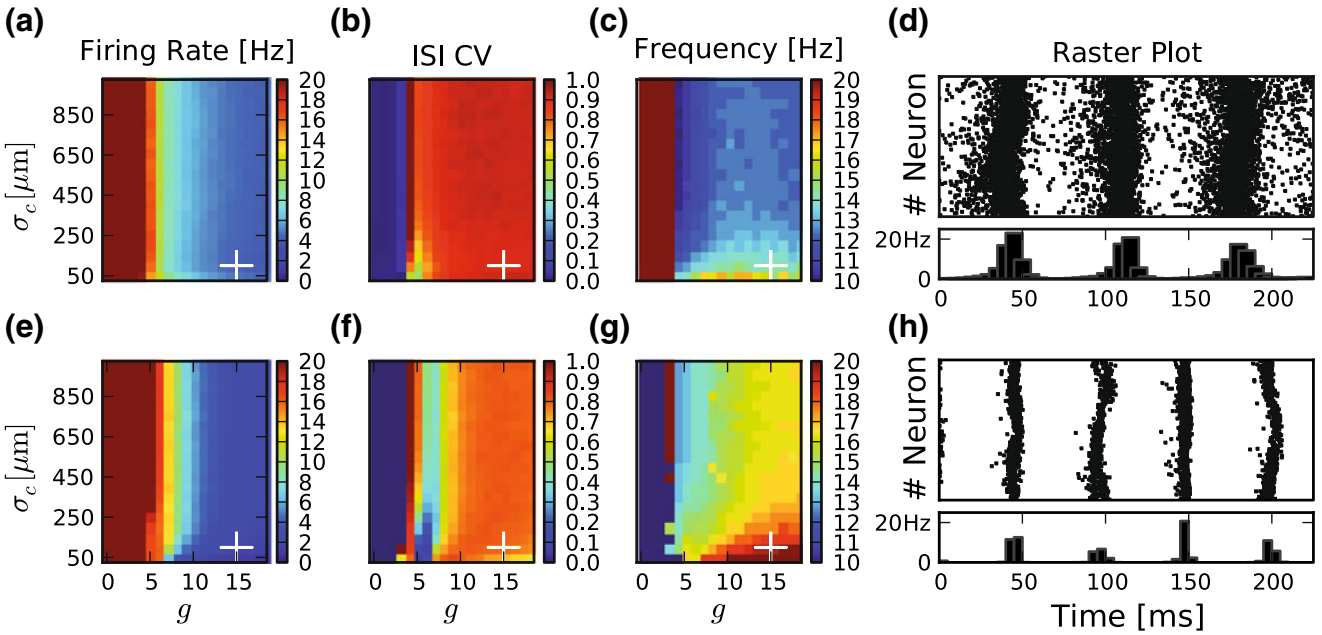

Fig. 3 Phase diagrams of the network statistics as a function of the local connectivity extent σ_c and the excitatory–inhibitory synaptic strength ratio g. (**a**)–(**c**) Phase diagram of the network with a connection density $\epsilon = 0.5\%$. (**a**) Mean firing rate, (**b**) mean CV ISI over the whole network, as a function of σ_c and g. (**c**) Mean frequency of the spontaneous oscillation generated in the population dynamics, as can be seen in the raster plot (all excitatory neurons, i.e 10,000 cells, (**d**)) of the activity for a particular regime ($g = 16$ and $\sigma_c = 100$ μm, *white cross*), and average firing rate with a 5 ms time bin. *Bottom*: (**e**)–(**h**) Same as in (**a**)–(**d**), but with a connection density $\epsilon = 5\%$

among those reported in Brunel (2000) and Mehring et al. (2003) for current-based synapses. We mainly focus on the states displayed in the raster plots of Fig. 3(d, h) where the network is in a slow Synchronous Irregular regime (SI) because we were interested in low firing rates and irregular activity. In such slow SI regimes, the network can display distinct waves of activity based on the underlying topology and delays. The spontaneous activity in sensory areas such as V1 is certainly irregular, and it is also known, with voltage sensitive dye imaging studies (Han et al. 2008; Contreras 2007; Arieli et al. 1996), that traveling waves appear and propagate. The slow SI regime seemed in that respect to be a good compromise to keep the irregularity and to promote the emergence of waves that mimic what is observed *in vivo*. To have a better insight, Fig. 4 shows distinct spatio-temporal profiles of the correlations in the case $\epsilon \in \{0.5\%, 5\%\}$ for two "extreme" connection spreads (top: $\sigma_c = 50$ μm, bottom: $\sigma_c = 500$ μm). One can clearly see the oscillations in the temporal domain due to the slow SI regime. Nevertheless, additional simulations shows that even in more asynchronous regimes, where correlations are less influenced by the structure and propagation waves are disrupted, our conclusions are still valid (see Supplementary Fig. 1). The same applies if we just increase the number of neurons, up to 100,000, without changing the connectivity: the density does not affect the result (see Supplementary Fig. 2).

To quantify the distance-dependent correlation profile in the network at the spiking level, we used two measures to distinguish the global amount of synchrony and the decrease as a function of distance. Figure 5(a) shows a typical profile of the pairwise cross-correlation as a function of distance. For each distance, we selected 2,000 pairs of neurons and averaged the Pearson correlation coefficient computed over all these pairs (see Section 2). These coefficients were computed between the corresponding spike trains and digitized with a time bin equal to the refractory period of the neurons, 5 ms. Supplementary Fig. 3 shows that for a larger time bin, the main results are qualitatively similar. The integrated correlation is defined as the integral over distances, and it reflects the global amount of synchrony present in the network. Figure 5(b) shows that on a log-log scale the decay of these pairwise correlations as a function of distance is approximately linear. The slope of this linear region will be referred to as the "correlation scaling exponent" obtained by a least square fit. A similar analysis can be performed at the membrane potential level: correlation coefficients at zero time-lag are used to assess the correlation between two membrane potentials, and the two measures

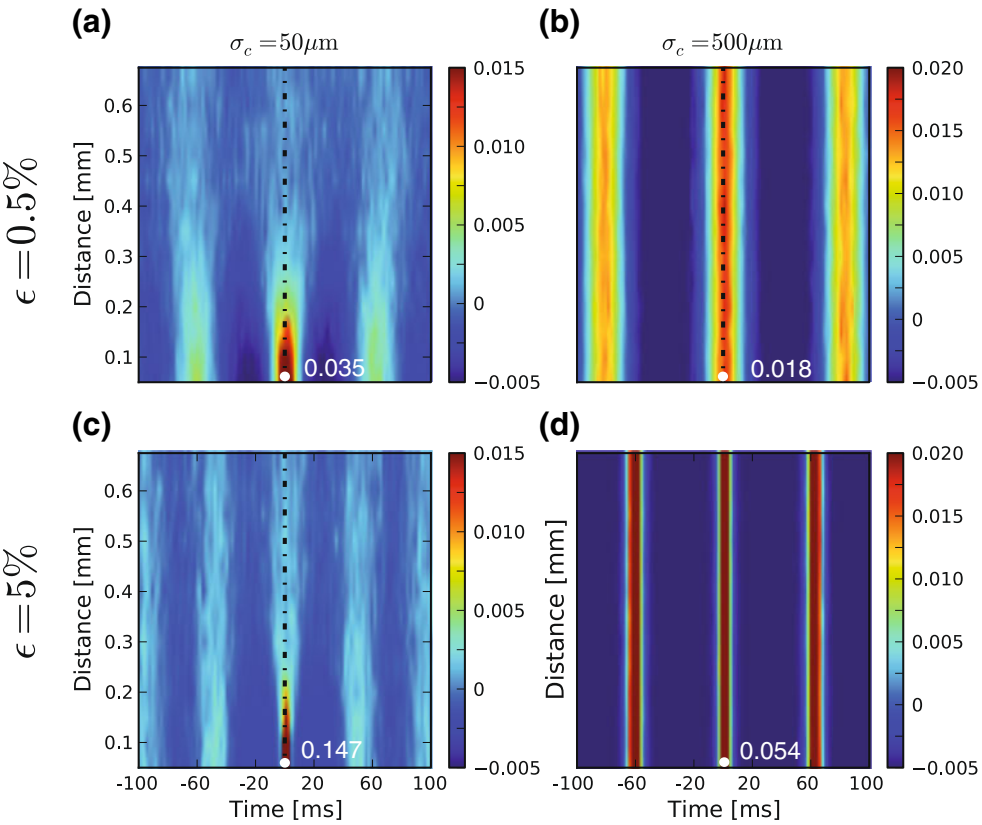

Fig. 4 Spatio-temporal profile of the spiking correlations in the network ($g = 16$) for two values of ϵ (*upper line* $\epsilon = 0.5\%$, *lower line* $\epsilon = 5\%$) and σ_c: 50 μm (*left*) (*upper panels* **a**, **b**), and 500 μm (*lower panels* **c**, **d**). *White dots* indicate the peak values of the instantaneous cross-correlations for nearby neurons

described in Section 2 and shown in Fig. 5 can also be applied.

The exhaustive analysis of these correlation profiles in the phase space previously explored in Fig. 3 is summarized in Fig. 6, for a connection density of $\epsilon = 0.5\%$. Qualitatively similar results can be obtained for the higher connection density (see Supplementary Fig. 4). The correlations have been analyzed both at

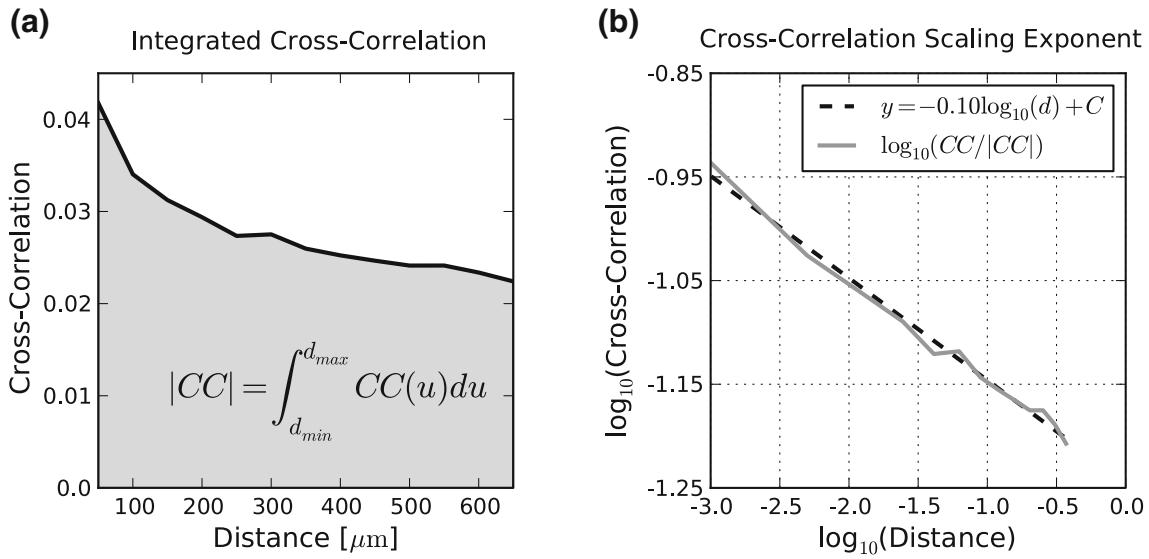

Fig. 5 Quantification of the distance-dependent correlation profile within the topological network. (**a**) Typical profile of spiking pairwise cross-correlation as a function of distance. The integrated correlation is the integral over all distances. (**b**) The correlation slope is fitted by a line on a log-log scale

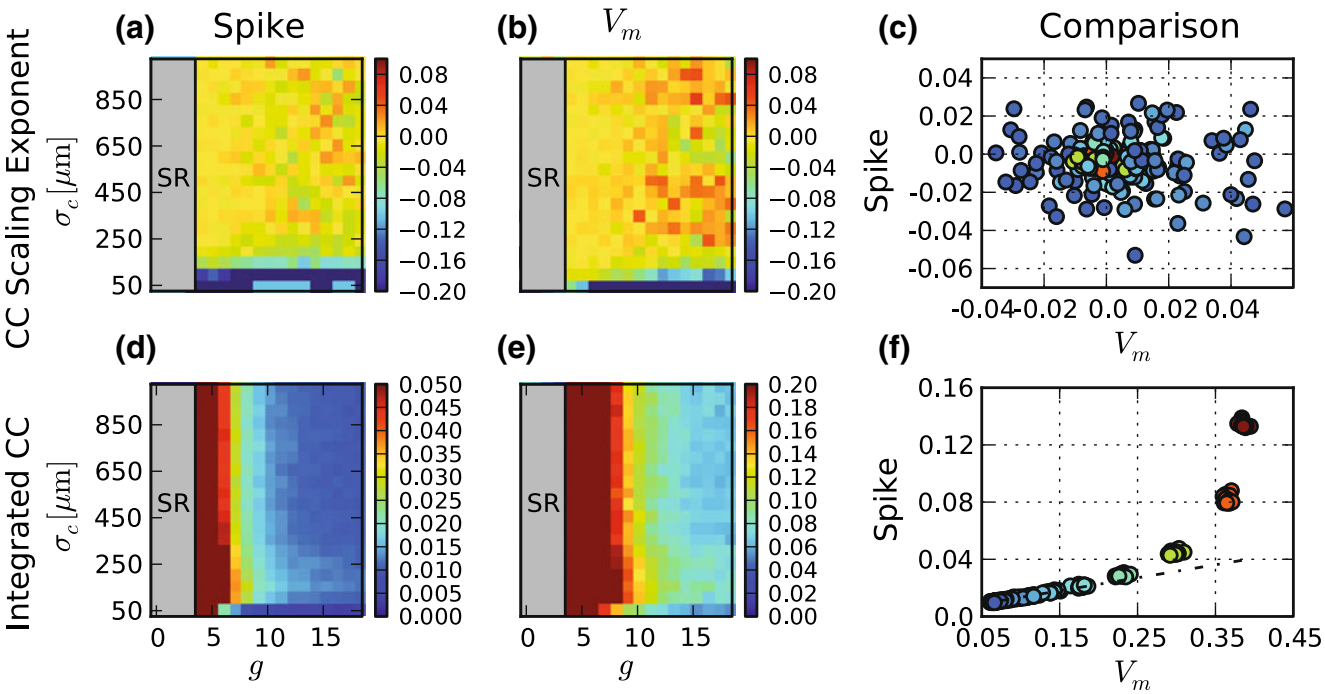

Fig. 6 Comparison of the distance-dependent correlations at the spiking and subthreshold (V_m) levels, for $\epsilon = 0.5\%$. (**a**), (**b**) Cross-correlation scaling exponent, analyzed either at the spiking level (**a**) or at the V_m level (**b**). (**c**) Cross-correlation scaling exponents at the V_m level (observed in panel (**b**)) plotted against values at the spiking level (observed in panel (**a**)). Same color-code as in Fig. 3, illustrating the firing rate of these particular points. (**d**), (**e**) Integrated correlations of the distance-dependent correlation profile, analyzed either at the spiking level (**d**) or at the V_m level (**e**). (**f**) Integrated correlations obtained at the V_m level (observed in panel (**d**)) plotted against the values obtained at the spiking level (observed in panel (**e**)). Same color-code

the spiking level and at the V_m level. In Fig. 6, panels a and d show the integrated correlation and correlation scaling exponent for correlations measured on spike trains, and panels b and e show these measures on membrane potentials. In both cases, one observes that the correlation scaling exponent does not depend on the connectivity parameters (see Fig. 6(a, b)). Except in the Synchronous Regular (SR) regime where large oscillations corrupt these measures, the scaling exponent is almost independent of σ_c and of the balance g and tends to zero on average. Figure 6(c) shows the values of the cross-correlation scaling exponent as measured on spike trains against values measured on the basis of V_m. Since both values are invariants, a uniform cloud of points is found without any particular statistical bias. In Fig. 6(d, e), one can see the integrated correlations, again measured on spike trains and on V_m. In both cases, the balance g dictates the amount of synchrony which is present in the network, in line with our previous results on averaged quantities. The more g is increased, the more dominant is the inhibition and the less synchronous is the network activity. By plotting the integrated cross-correlations measured at the spiking level against those recorded at the V_m level (Fig. 6(f)), we can see that for low rate regimes, the relation between the integrated spiking correlation and the sub-threshold correlation is almost linear and then increases in a nonlinear and monotonic manner for higher firing rates. The clusters are isolated according to the network firing rate shown in color code identical to the one used in Fig. 3. Therefore, in these network configurations, the integrated correlation measured at the subthreshold level is uniquely determined by the spiking correlation.

To study the influence of heterogeneity in the connection scheme, the ratio between the spread of the Gaussian profile used to connect the excitatory and the inhibitory neurons within the network was varied. Figure 7(a) illustrates how these two parameters σ_{exc} and σ_{inh} were changed. Instead of exploring the whole parameter space, only two lines were explored: one with σ_{exc} fixed to 200 μm while σ_{inh} was varied in the range 0–1 mm, and another where σ_{exc} was varied for a fixed σ_{inh} (respectively red and blue curves in Fig. 7). As can be seen in the Fig. 7(b–f), averaged quantities such as mean firing rate, population peak oscillatory frequency, or mean ISI CV are hardly affected by these parameters, provided σ_{exc} or σ_{inh} are not too small. If they are, one can observe a symmetry breaking pushing the network into pathological states (Fig. 7(d–h)) with

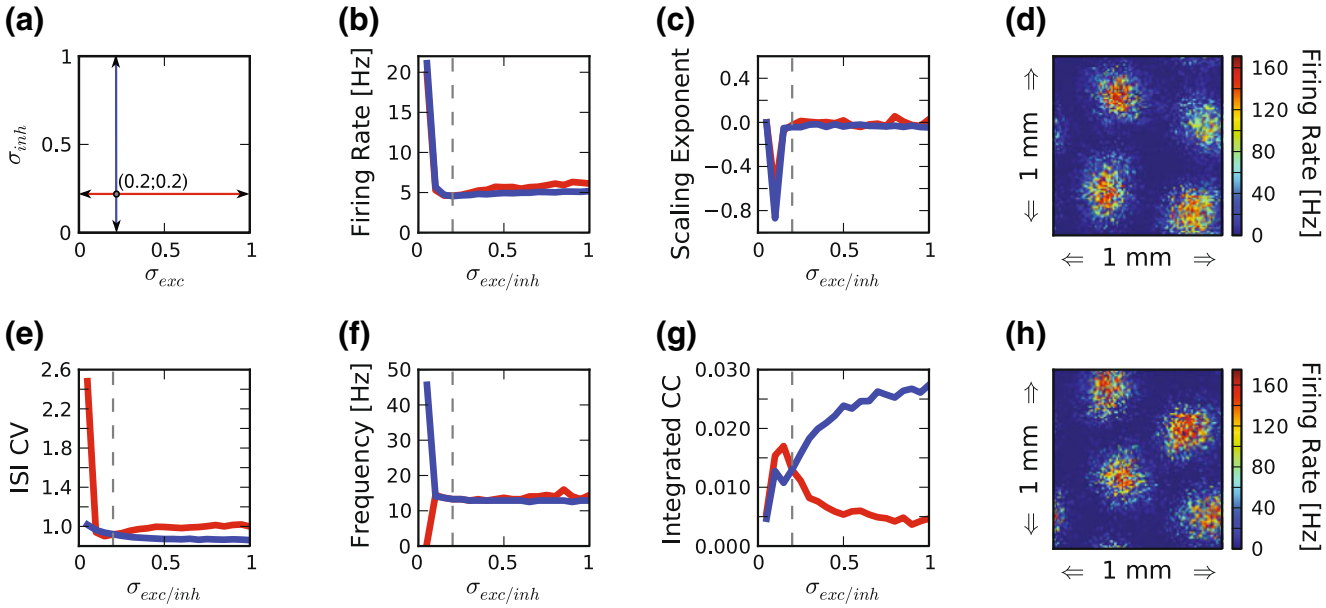

Fig. 7 Changing the spatial spread σ_c of the excitatory and inhibitory connections independently. (**a**) Schematic illustration explaining the parameter region explored. In *red*, σ_{inh} is held constant while σ_{exc} is varied, while in *blue*, the opposite. In all subsequent panels (**b**, **c**, **e**–**g**), the intersection point is represented by the *dashed gray line*. (**b**) Mean firing rate, (**c**) cross-correlation scaling exponent, (**f**) population activity peak frequency, (**e**) mean ISI CV and (**g**) integrated correlations as a function of σ_{exc} or σ_{inh}. (**d**), (**h**) Time-averaged activity maps of the two pathological cases that emerged for low σ_{exc} (**d**) or σ_{inh} (**h**) values

very localized bumps of activity spontaneously jumping from one state to another. This scenario is reminiscent of the "hotspots"-like patterns obtained by Usher et al. (1994) with a Mexican-hat connectivity profile and hybrid neurons violating Dale's principle (i.e both exciting and inhibiting their target cells (Kriener et al. 2008)). Our finding of Turing-type patterns resulting from differences in connectivity together with the non-linearity of the system is thus compatible with their model when the network connectivity is local enough to generate strong topological correlations. Otherwise, one can again notice that the cross-correlation scaling exponent is rather insensitive to the connectivity spatial spread and close to zero (Fig. 7(c)), while the integrated cross-correlation is affected by the spread (Fig. 7(g)). Increasing the spread of inhibitory projections while keeping that of excitatory neurons constant increases the overall amount of synchrony within the network, by diluting the inhibition. On the other hand, increasing the spread of the excitation by keeping fixed that of inhibition decreases the amount of synchrony by diluting excitation.

Finally, we explored the role of propagation delays and their influence on the spatial spread of distance-dependent cross-correlations within the network. In particular, we studied the impact of propagation speed for different network structure parameters: the connection spatial spread and the connection density. For highly localized connectivity ($\sigma_c = 50$ μm, Fig. 8(a, c)) changing the speed has no significant effect on the correlation profile, for both low and high connectivity densities. Indeed, when only nearby neurons are connected, the effective delays for various velocities are still small enough to leave the profiles unaffected. Similarly, when a larger Gaussian profile is used in a network with high connectivity density ($\epsilon = 5\%$, $\sigma_c = 200$ μm, see Fig. 8(d)), we found that changing the velocity induces a higher variability in the correlation profiles, without any consistent variation. However, when considering large connectivity spread in very diluted networks, where the propagation delays become crucial ($\epsilon = 0.5\%$, $\sigma_c = 200$ μm, see Fig. 8(c)), the integrated correlation increases with velocity. It has to be stressed that the case $\sigma_c = 50$ μm in Fig. 8(a, c) is a limit case, because the network is close to a pathological state where the neurons are almost densely connected in an all-to-all nearest-neighbor connection scheme (see inset of Fig. 1(c)). These very localized connections establish differences with broader σ_c. The fact that the bottom rows of Fig. 6(a, b, d, e) (for $\sigma_c < 100$ μm) are different is consistent with the observation that in Fig. 8 there is a clear difference, for fixed ϵ, in the correlations for the two values of σ_c used. In fact, one has to keep in mind that the shapes of the curves in Fig 8(a, c) are

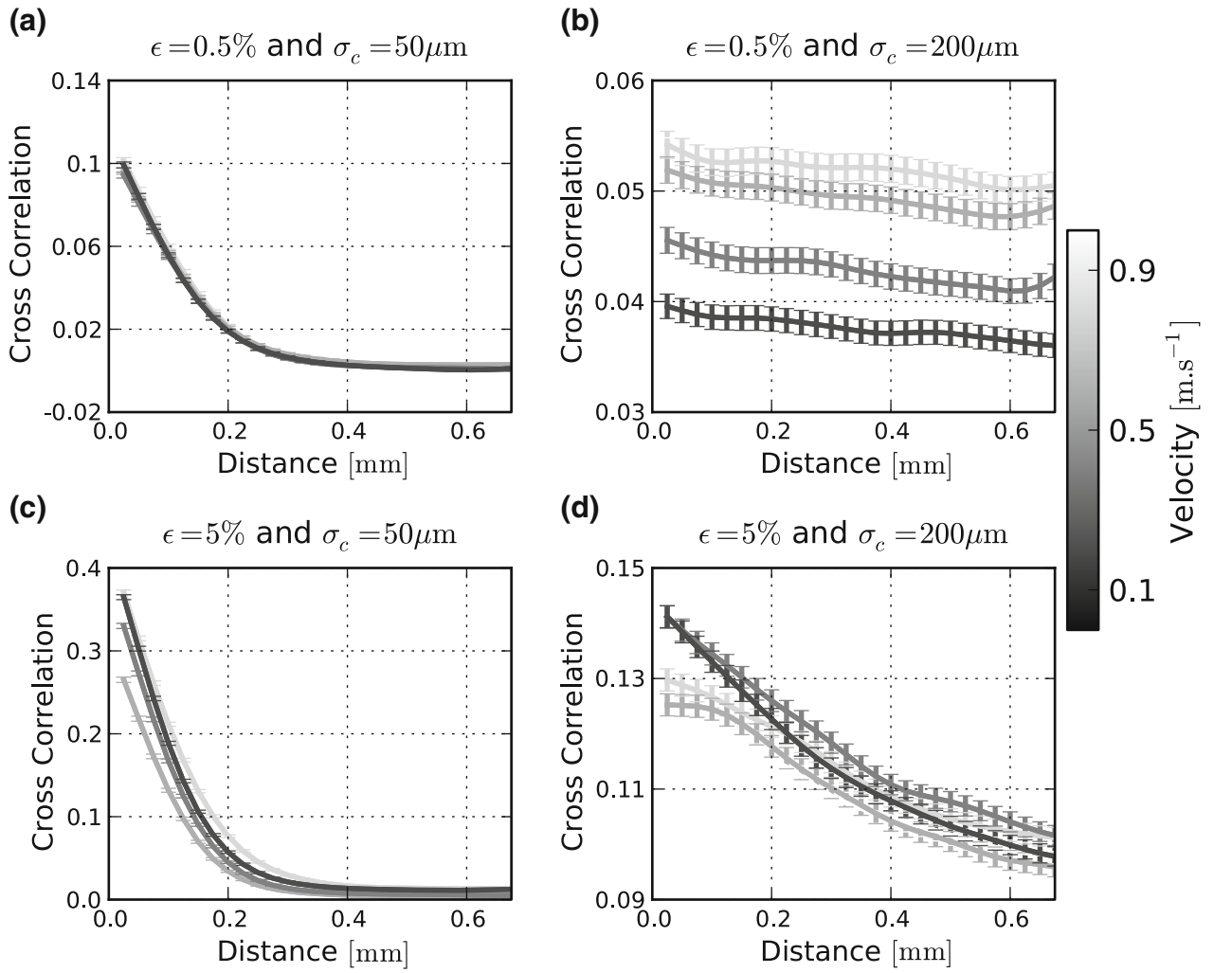

Fig. 8 Influence of delays on the cross-correlation profiles. The average pairwise Pearson correlation coefficient is plotted in a network with a connectivity density $\epsilon = 0.5\%$, as a function of the distance within neuronal pairs, for four distinct velocity values. *Error bars* show the standard error of the mean. Two Gaussian profiles are considered. (**a**) A very local one ($\sigma_c = 50\mu$m). (**b**) A broader one ($\sigma_c = 200\mu$m). (**c**), (**d**) Same as (**a**) and (**b**), but in a denser network with $\epsilon = 5\%$

valid only for very local networks ($\sigma_c = 50$ μm), and that in all the other configurations ($\sigma_c > 100$ μm), the curves would look like those in Fig 8(b, d)). Altogether, we conclude that propagation delays have a significant effect on the spatial correlation profile only when long-range interactions are as important as local interactions. The linear relationship between delays and distances used in the model can be considered as too strong. Indeed, for a very dense and intricate circuit, such as the one studied in Oswald and Reyes (2008), this relationship is not that obvious. If there is evidence that conduction times within dendrites and/or axons are linear, this linearity due to the wiring scheme may be more noisy than in our model. Nevertheless, we checked that the invariance and the results are still valid when delays and distances are linearly correlated, but are not related by a unique functional relationship anymore, such as $d_{ij} = d_{\text{syn}} + \frac{r_{ij}}{v}(1 + \mathcal{N}(0, \sigma))$, where $\mathcal{N}(0, \sigma)$ is Gaussian noise of variance $\sigma = 0.25$ (see Supplementary Fig. 5).

5 Effect of structured stimulation

Having studied the response of the network under unstructured stimulation (Poissonian input, mimicking the spontaneous ongoing activity coming from the thalamus), we were interested in adding an additional layer to inject spatial correlations (representing the sensory drive) in the network. More precisely, we simulated a layer of Poisson sources arranged also in a 2D

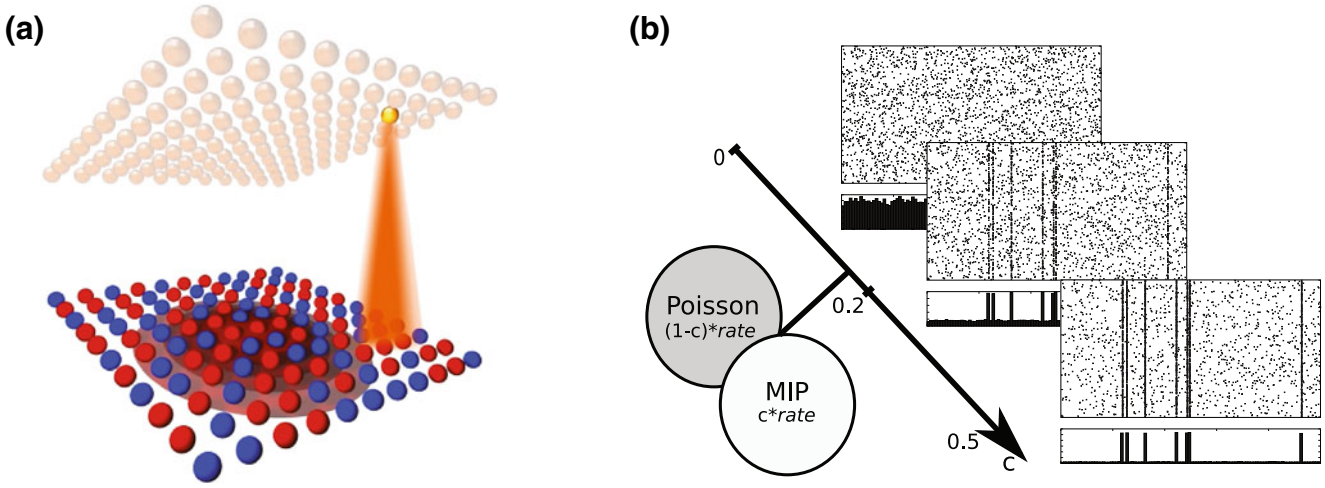

Fig. 9 Schematic view of the input layer used to inject spatial correlations. (**a**) An additional 2D layer of sources is added, where each excitatory source connects to the recurrent network with a Gaussian profile of standard deviation σ_{ext} in a divergent manner (taken from El Boustani et al. 2009). (**b**) Illustration of the compound process made with Multiple Interaction and Poisson processes, shown as raster plots of the activity for 2,500 cells in the external layer, for several values of c. The parameter c controls the percentage of co-active neurons into synchronous volleys

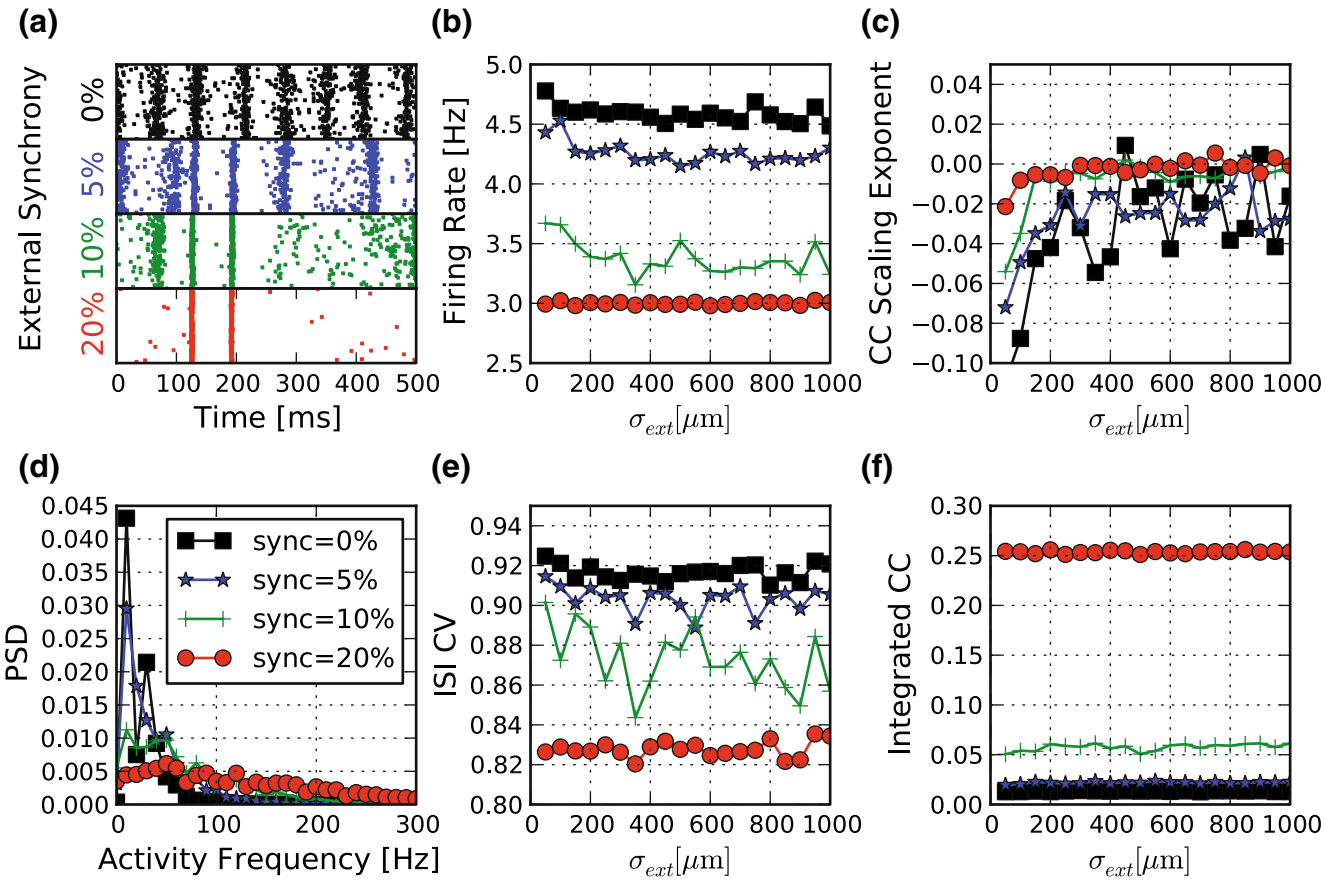

Fig. 10 Evoked activity under spatially correlated stimulation for $\epsilon = 0.5\%$. (**a**) Three raster plots for 2,500 neurons and different synchrony levels in the input. (**b**) Mean firing rate, (**c**) cross-correlation scaling exponent, (**e**) mean CV ISI and (**f**) integrated correlation in the recurrent network as a function of the input divergence σ_{ext}, for the four levels of synchrony. (**d**) Power spectra density for a fixed $\sigma_{\text{ext}} = 200$ μm and the four levels of synchrony

plane (Fig. 9(a)), connected to the recurrent network with a divergent Gaussian spread with a variance σ^2_{ext}, and acting as compound processes made with Poisson sources and Multiple Interaction Processes (Kuhn et al. 2003) (MIP). To be more precise, c is the percentage of neurons that will emit simultaneous spikes during some volleys, appearing at a frequency $c\nu_{\text{ext}}$. The MIP is a process of thinning a Poisson "mother" spike train at a frequency ν_{ext} to obtain a set of daughter trains by duplication of the spikes with a probability c, so that the daughters have rates $c\nu_{\text{ext}}$ and pairwise correlation c. By using the compound of the MIP and independent Poissonian sources at a frequency $(1-c)\nu_{\text{ext}}$, each external cell acts therefore as an excitatory source, sharing global inputs imposed by the MIP at a frequency $c\nu_{\text{ext}}$. The combination of these two processes allowed us to control, with a continuous parameter $c \in [0, 1]$ (Fig. 9(b)), the amount of synchrony sent to the network while keeping the mean input firing rate ν_{ext} constant.

Figure 10 shows the response of the network for four external input synchrony levels $c \in \{0, 0.05, 0.1, 0.2\}$, and for different spreads of the external input divergence σ_{ext}. In Fig. 10(a), four typical raster plots are represented for these four levels of synchrony with an identical external input rate fixed at 5 spikes/s (as in the unstructured case). The more c is increased, the more efficiently the synchrony will trigger strong responses in the recurrent network, while, at the same time, decreasing the general firing rate by forcing every neuron in their refractory period (Fig. 10(b)). For averaged quantities such as the mean firing rate and CV ISI (Fig. 10(b, e)), the external divergence σ_{ext} of the feedforward projection does not have any influence, a phenomenon already observed in the presence of unstructured inputs. Increasing the external synchrony will broaden the spectral responses and decrease the frequency content of the oscillatory activity in the population dynamics because of the stochastic nature of the input (Fig. 10(d)). Regarding the correlation profile as a function of distance, increasing the synchrony c induces an increase in the integrated correlation of the recurrent network (Fig. 10(f)), but more importantly, we observed that the external correlation is now able to change the correlation scaling exponent of the distance-dependent correlation profile, especially when the external connectivity spread is narrow (Fig. 10(c)).

These changes are summarized in Fig. 11, where we chose $\sigma_{\text{ext}} = 50$ μm for the sake of clarity. In Fig. 11(a), one can observe the increase in the integrated correlations following an increase of the external synchrony. The more the network receives strong synchronous spiking volleys, the stronger are the pairwise correlation coefficients. As one can see in Fig. 11(b), increasing the external synchrony also affects the cross-correlation scaling exponent of the distance-dependent correlation profile. Adding synchrony favors synchronous volleys that are strong enough to trigger spiking activity in the recurrent network at any position simultaneously. This global activation pattern in turn creates

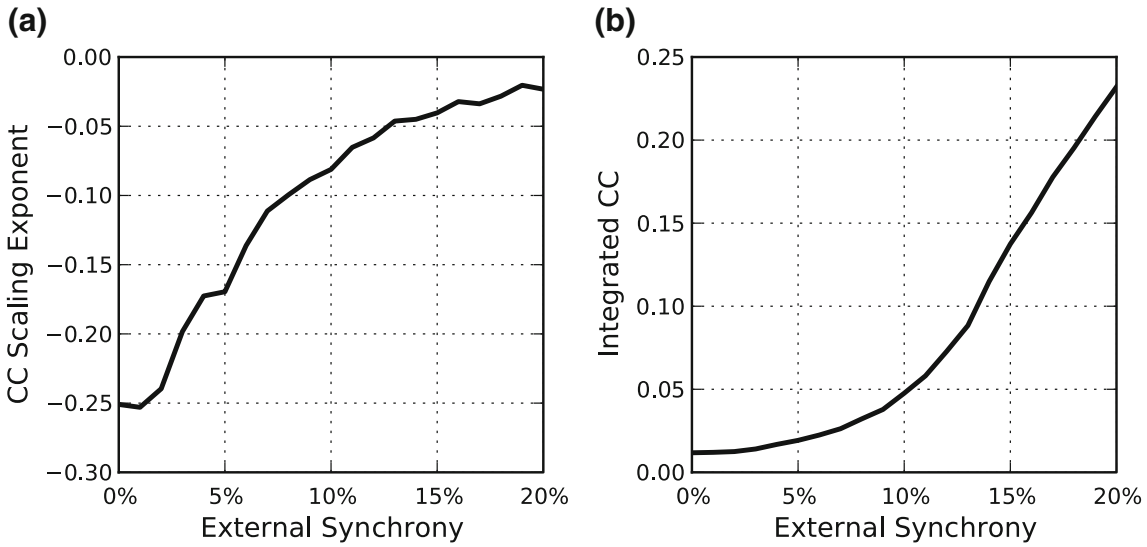

Fig. 11 Change in the distance-dependent correlation profile as a function of the level of synchrony in the input for $\epsilon = 0.5\%$. (**a**) Correlation scaling exponent in the recurrent network as a function of the external synchrony. (**b**) Integrated correlation in the stimulated layer as a function of the external synchrony

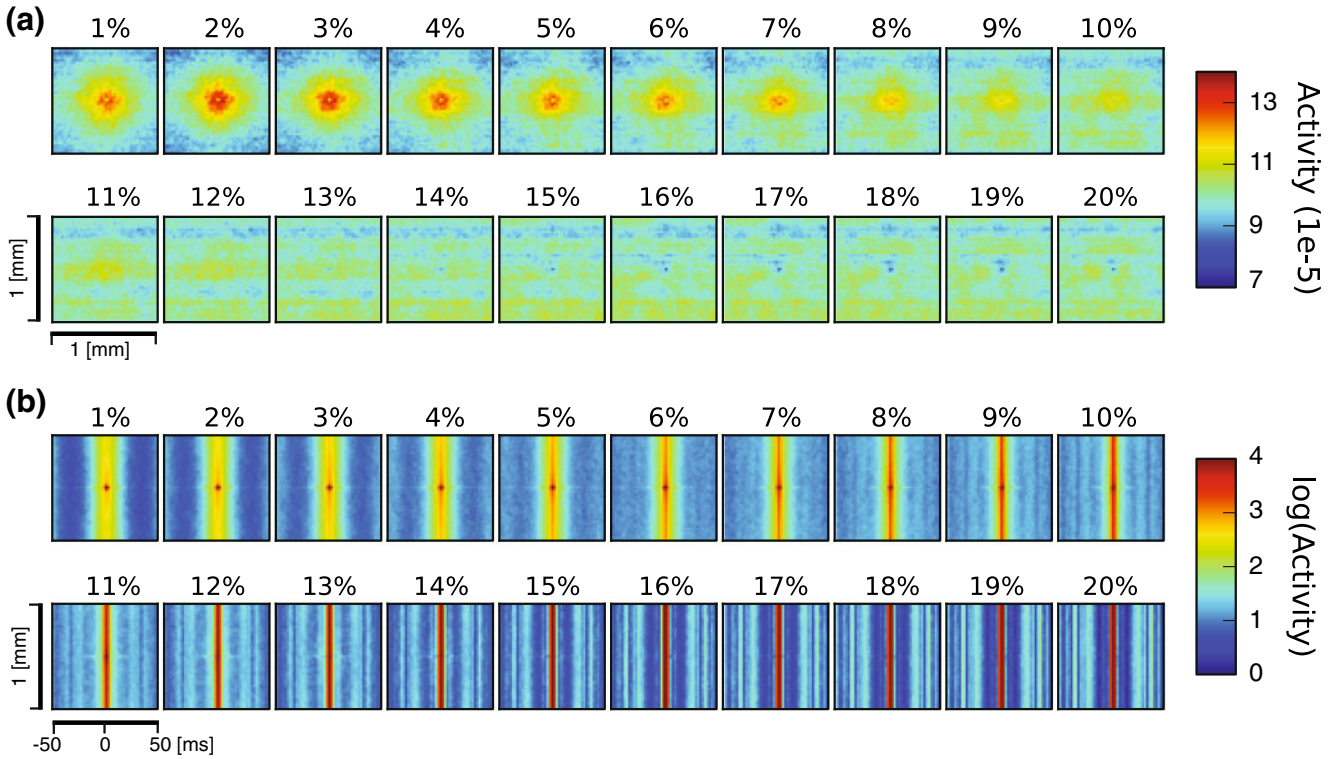

Fig. 12 Network activity spike-triggered average (NASTA) as a function of external synchrony for $\epsilon = 0.5\%$. (**a**) NASTA for one neuron. The maps show the spatial network activity averaged over all its spikes, 2 ms before, for several level of external synchrony. (**b**) Same as in (**a**), but the activity is now plotted only for the central spatial line of the map and as a function of time

long-range correlations in the network. Conversely, for narrow stimulation spatial spread without any additional spatial correlations (no synchrony), small assemblies of neurons become strongly correlated in a spatial range shorter than that observed in the spontaneous activity.

The genesis of these processes can be better understood by studying the presynaptic patterns leading to spikes, called network activity spike-triggered average (NASTA). This is shown in Fig. 12(a), where the recurrent inputs are mainly responsible for the emission of a spike for low levels of external synchrony. The fact that a localized PSTH is obtained for $c < 10\%$ means that the network activity of the surrounding neurons 2 ms earlier will be driving the post-synaptic neuron to spike. The more c is increased, the less important is the recurrent connectivity contribution and the stronger are the external spiking volleys to trigger by themselves a spike. In the NASTA spatio-temporal domain (Fig. 12(b)), one can see that the broad temporal spread around the postsynaptic neuron accounts for the propagation delay with the presynaptic neurons in the network. Here again, the external spike volleys have a role in flattening the spatial correlation and sharpening the temporal spread of cross-correlation when increasing the external synchrony.

6 Discussion

Invariant macroscopic statistics In this paper, we have studied balanced network models with conductance-based synaptic interactions and different spatial profiles of connectivity. Our main finding is that such balanced networks possess connectivity-invariant quantities as long as each neuron is sparsely connected to its neighbors. Surprisingly, this result holds even for very narrow Gaussian connectivity. This is a very encouraging result which shows that mean-field approaches, where no topology is taken into account, can offer a reliable description of the network at macroscopic scales as long as the dynamical regime of conductances remains stationary and homogenous across the network.

For instance, when modeling data such as voltage-sensitive dyes imaging (VSDI) recordings, there is a priori no need to know the fine details of the connectivity within each pixel. In particular, we know that for

the spontaneous activity regime, the mean firing rate, the mean CV ISI and the overall synchrony depend mainly on the synaptic E/I balance ratio (except for the first-neighbor extreme case). We also observed that the spatial correlation decay in this regime depends neither on the connectivity extent nor on the conductance balance in the irregular regime. However, we do see a dependency of the correlation decay on the connectivity density (which is anyway a structural averaged quantity).

Similar conclusions apply to the case of networks subject to structured input (representing external correlation patterns imposed by the sensory drive). We showed that the fine details of the connectivity are less influential than averaged quantities such as the overall synchrony. It should therefore be possible to find a simple relation describing the spatial correlation decay only in terms of macroscopic quantities such as the mean synaptic input per neuron or the mean synchrony in the external drive.

We observed numerically that most of the first- and second-order statistics in these networks are ruled by averaged macroscopic structural quantities. Therefore, it seems that for these models, structural (synaptic weights, mean synaptic input) and dynamical (mean firing rate, correlations) statistics are related to each other in a hierarchical manner, as already observed in a simpler setting (Liu and Nykamp 2009). We therefore do not conclude that connectivity is completely "decoupled" from correlation, but rather that this detail of description is irrelevant at a large-scale level of observation. The underlying mechanistic explanation is directly linked to the way these balanced activities are generated in sparse networks, and we show how these dynamics break in the extreme case of dense local connectivity.

Supra- and sub-threshold correlations Several studies have focused recently on the second-order transfer function of spiking neurons. More precisely, knowing the correlation structure in the presynaptic activity of one or two neurons sharing a common input, one can ask what is the spiking auto-correlation of each neuron and/or their cross-correlation. It has been shown recently that for the low-correlation regime, the supra- and sub-threshold activities are linearly related with a proportionality factor which mainly depends on the firing rate of these neurons (de la Rocha et al. 2007; Shea-Brown et al. 2008). In our situation, conclusions are harder to reach from an analytical point of view, because we are considering populations of neurons. However, we found a monotonic relation between the supra- and sub-threshold signal correlation proving that both levels offer a similar description of the correlation state in the network. For spontaneous activity (uncorrelated inputs), these correlations are generated by the recurrent connections within the network, so that this monotonic relation must satisfy a self-consistent relation in order to be stable. Describing this relation through closed analytical equations for simpler models would bring us a step further in the understanding of recurrent network dynamics.

Comparison with other studies Previous studies have aimed to describe the relationship between network structure and dynamics. For example in Usher et al. (1994), the authors studied networks displaying irregular spiking activity and long-range temporal correlations. They reported that in a small network with "hybrid" neurons violating Dale's principle (Kriener et al. 2008), and connected in a Mexican hat manner (local excitation and long-range inhibition), they were able to generate network dynamics with a high degree of variability. However, their network regime was not balanced, and the irregular activity in the network was generated by "hotspot"-type activity patterns (similar to those described in Fig. 7(d–h)), instead of waves. In Kitano and Fukai (2007), the authors report that in small and highly clustered small-world networks, the spiking irregularity is strongly dependent on the synaptic weight balance and the small-world rewiring parameter. However, this approach is far from the sparse connectivity we are considering here, and it does not match the mean-field requirements for a suitable prediction of macroscopic dynamical quantities. Nevertheless, in their computation of distance-dependent correlation and beyond the local region, there is a large region where the correlation scaling exponent does not depend as strongly on the connectivity scheme (see Fig. 5 of Kitano and Fukai 2007).

Shaping the correlation landscape with correlated input When the network was fed with uncorrelated input, it was not possible to change the distance-dependent correlation scaling exponent by changing the connectivity extent or the synaptic weight ratio. However, changing the connectivity density or the correlations in the input either broadens or shortens the distance-dependent correlations. This could be also easily seen through the network activity spike-triggered average where the correlation landscape becomes uniform in space and narrow in time by increasing synchrony. Taken together with the fact that spiking and sub-threshold correlations have a monotonic relationship, this could be a way to estimate the impact of sensory input on ongoing activity

using measurements such as VSD imaging, single-cell unit activity, or local field potentials.

Acknowledgements We thank Olivier Marre for helpful discussions and Andrew Davison for comments on the manuscript. P.Y. was supported by a MENRT bursary from the University of Paris XI, S.E.B was supported by a FRM fellowship. Research supported by the CNRS, ANR (NATSTATS and HR-CORTEX) and the European Commission (FACETS FP6-2004-IST-FETPI 15879 and Brain-i-Nets FP7-ICT-2007-C 243914).

References

Amit, D. J., & Brunel, N. (1997). Model of global spontaneous activity and local structured activity during delay periods in the cerebral cortex. *Cerebral Cortex, 7*(3), 237–252.

Arieli, A., Sterkin, A., Grinvald, A., & Aertsen, A. (1996). Dynamics of ongoing activity: Explanation of the large variability in evoked cortical responses. *Science, 273*(5283), 1868–1871.

Benucci, A., Frazor, R. A., & Carandini, M. (2007). Standing waves and traveling waves distinguish two circuits in visual cortex. *Neuron, 55*(1), 103–117.

Berger, D., Warren, D., Normann, R., Arieli, A., & Grün, S. (2007). Spatially organized spike correlation in cat visual cortex. *Neurocomputing, 70*(10–12), 2112–2116.

Bienenstock, E. (1996). On the dimensionality of cortical graphs. *Journal of Physiology (Paris), 90*(3–4), 251–256.

Braitenberg, V, & Schüz, A. (1998). *Cortex: Statistics and geometry of neuronal connectivity*. Berlin: Springer.

Bringuier, V., Chavane, F., Glaeser, L., & Frégnac, Y. (1999). Horizontal propagation of visual activity in the synaptic integration field of area 17 neurons. *Science, 283*(5402), 695–699.

Brunel, N. (2000). Dynamics of sparsely connected networks of excitatory and inhibitory spiking neurons. *Journal of Computational Neuroscience, 8*(3), 183–208.

Cessac, B., & Viéville, T. (2008). On dynamics of integrate-and-fire neural networks with conductance based synapses. *Frontiers Computational Neuroscience, 2*, 2. doi:10.3389/neuro.10.002.2008.

Contreras, D. (2007). Propagating waves in visual cortex. *Neuron, 55*(1), 3–5.

Davison, A. P., Bruederle, D., Eppler, J., Kremkow, J., Muller, E., Pecevski, D., et al. (2009) PyNN: A common interface for neuronal network simulators. *Front Neuroinformatics 2*, 11. doi:10.3389/neuro.11.011.2008.

de la Rocha, J., Doiron, B., Shea-Brown, E., Josi, K., & Reyes, A. (2007). Correlation between neural spike trains increases with firing rate. *Nature, 448*(7155), 802–806.

Destexhe, A, & Paré, D. (1999). Impact of network activity on the integrative properties of neocortical pyramidal neurons *in vivo*. *Journal of Neurophysiology, 81*(4), 1531–1547.

Diesmann, M., & Gewaltig, M. (2001). NEST: An environment for neural systems simulations. *Forschung und wisschenschaftliches Rechnen, Beitrage zum Heinz-Biling-Preis 58*, 43–70.

El Boustani, S., & Destexhe, A. (2009). A master equation formalism for macroscopic modeling of asynchronous irregular activity states. *Neural Computation, 21*(1), 46–100.

El Boustani, S., Marre, O., Béhuret, S., Baudot, P., Yger, P., Bal, T., et al. (2009). Network-state modulation of power-law frequency-scaling in visual cortical neurons. *PLoS Computational Biology, 5*(9), e1000,519.

Gil, Z., Connors, B. W., & Amitai, Y. (1999). Efficacy of thalamocortical and intracortical synaptic connections: Quanta, innervation, and reliability. *Neuron, 23*(2), 385–397.

Gilbert, C. D., & Wiesel, T. N. (1983). Clustered intrinsic connections in cat visual cortex. *Journal of Neuroscience, 3*(5), 1116–1133.

Göbel, W., Kampa, B. M., & Helmchen, F. (2007). Imaging cellular network dynamics in three dimensions using fast 3D laser scanning. *Nature Methods, 4*(1), 73–79.

Gonzlez-Burgos, G., Barrionuevo, G., & Lewis, D. A. (2000). Horizontal synaptic connections in monkey prefrontal cortex: An *in vitro* electrophysiological study. *Cerebral Cortex, 10*(1), 82–92.

Greenberg, D. S., Houweling, A. R., & Kerr, J. N. D. (2008). Population imaging of ongoing neuronal activity in the visual cortex of awake rats. *Nature Neuroscience, 11*(7), 749–751.

Grinvald, A., Lieke, E. E., Frostig, R. D., & Hildesheim, R. (1994). Cortical point-spread function and long-range lateral interactions revealed by real-time optical imaging of macaque monkey primary visual cortex. *Journal of Neuroscience, 14*(5 Pt 1), 2545–2568.

Han, F., Caporale, N., & Dan, Y. (2008). Reverberation of recent visual experience in spontaneous cortical waves. *Neuron, 60*(2), 321–327.

Hellwig, B. (2000). A quantitative analysis of the local connectivity between pyramidal neurons in layers 2/3 of the rat visual cortex. *Biological Cybernetics, 82*(2), 111–121.

Izhikevich, E. M., Gally, J. A., & Edelman, G. M. (2004). Spike-timing dynamics of neuronal groups. *Cerebral Cortex, 14*(8), 933–944.

Kitano, K., & Fukai, T. (2007). Variability v.s. synchronicity of neuronal activity in local cortical network models with different wiring topologies. *Journal of Computational Neuroscience, 23*(2), 237–250.

Kohn, A., & Smith, M. A. (2005). Stimulus dependence of neuronal correlation in primary visual cortex of the macaque. *Journal of Neuroscience, 25*(14), 3661–3673.

Kriener, B., Tetzlaff, T., Aertsen, A., Diesmann, M., & Rotter, S. (2008). Correlations and population dynamics in cortical networks. *Neural Computation, 20*(9), 2185–2226.

Kriener, B., Helias, M., Aertsen, A., & Rotter, S. (2009). Correlations in spiking neuronal networks with distance dependent connections. *Journal of Computational Neuroscience, 27*(2), 177–200.

Kuhn, A., Aertsen, A., & Rotter, S. (2003). Higher-order statistics of input ensembles and the response of simple model neurons. *Neural Computation, 15*(1), 67–101.

Kumar, A., Schrader, S., Aertsen, A., & Rotter, S. (2008), The high-conductance state of cortical networks. *Neural Computation, 20*(1), 1–43.

Larkum, M. E., Zhu, J. J., & Sakmann, B. (2001). Dendritic mechanisms underlying the coupling of the dendritic with the axonal action potential initiation zone of adult rat layer 5 pyramidal neurons. *Journal of Physiology, 533*(Pt 2), 447–466.

Liu, C. Y., & Nykamp, D. Q. (2009). A kinetic theory approach to capturing interneuronal correlation: The feedforward case. *Journal of Computational Neuroscience, 26*, 339–368.

Marre, O., Yger, P., Davison, A., & Frégnac, Y. (2009). Reliable recall of spontaneous activity patterns in cortical networks. *Journal of Neuroscience, 29*(46), 14596–14606.

Mehring, C., Hehl, U., Kubo, M., Diesmann, M., & Aertsen, A. (2003). Activity dynamics and propagation of synchronous spiking in locally connected random networks. *Biological Cybernetics, 88*(5), 395–408.

Mitchell, J. F., Sundberg, K. A., & Reynolds, J. H. (2009). Spatial attention decorrelates intrinsic activity fluctuations in macaque area v4. *Neuron, 63*(6), 879–888.

Nauhaus, I., Busse, L., Carandini, M., & Ringach, D. L. (2009). Stimulus contrast modulates functional connectivity in visual cortex. *Nature. Neuroscience, 12*(1), 70–76.

Nirenberg, S., & Latham, P. E. (2003). Decoding neuronal spike trains: How important are correlations? *Proceedings of the National Academy of Sciences of the United States of America, 100*(12), 7348–7353.

Oswald, A. M. M., & Reyes, A. D. (2008). Maturation of intrinsic and synaptic properties of layer 2/3 pyramidal neurons in mouse auditory cortex. *Journal of Neurophysiology, 99*(6), 2998–3008.

Renart, A., de la Rocha, J., Bartho, P., Hollender, L., Parga, N., Reyes, A., et al. (2010). The asynchronous state in cortical circuits. *Science, 327*(5965), 587–590.

Roxin, A., Brunel, N., & Hansel, D. (2005). Role of delays in shaping spatiotemporal dynamics of neuronal activity in large networks. *Physical Review Letters, 94*(23), 238103.

Schwarz, C., & Bolz, J. (1991). Functional specificity of a long-range horizontal connection in cat visual cortex: A cross-correlation study. *Journal of Neuroscience, 11*(10), 2995–3007.

Shea-Brown, E., Josi, K., de la Rocha, J., & Doiron, B. (2008). Correlation and synchrony transfer in integrate-and-fire neurons: Basic properties and consequences for coding. *Physical Review Letters, 100*(10), 108102.

Singer, W., & Gray, C. M. (1995). Visual feature integration and the temporal correlation hypothesis. *Annual Review of Neuroscience, 18*, 555–586.

Smith, M. A., & Kohn, A. (2008). Spatial and temporal scales of neuronal correlation in primary visual cortex. *Journal of Neuroscience, 28*(48), 12591–12603.

Usher, M., Stemmler, M., Koch, C., & Olami, Z. (1994). Network amplification of local fluctuations causes high spike rate variability, fractal firing patterns and oscillatory local field potentials. *Neural Computation, 6*(5), 795–836.

van Vreeswijk, C., & Sompolinsky, H. (1996). Chaos in neuronal networks with balanced excitatory and inhibitory activity. *Science, 274*(5293), 1724–1726.

van Vreeswijk, C., & Sompolinsky, H. (1998). Chaotic balanced state in a model of cortical circuits. *Neural Computation, 10*(6), 1321–1371.

Vogels, T. P., & Abbott, L. F. (2005). Signal propagation and logic gating in networks of integrate-and-fire neurons. *Journal of Neuroscience, 25*(46), 10786–10795.

Voges, N., Aertsen, A., & Rotter, S. (2007). Statistical analysis of spatially embedded networks: From grid to random node positions. *Neurocomputing, 70*(10–12), 1833–1837.

Zohary, E., Shadlen, M. N., & Newsome, W. T. (1994). Correlated neuronal discharge rate and its implications for psychophysical performance. *Nature, 370*(6485), 140–143.